ORIGINAL PAPER

Dynamics and manipulation of Airy beam in fractional system with diffraction modulation and PT-symmetric potential

Xiaoqin Bai · Rongcao Yang (iD) **· Heping Jia · Juan Bai**

Abstract We investigate the dynamics and manipulation of finite energy Airy (FEA) beam in fractional system with diffraction modulation and PT-symmetric potential. In the absence of PT-symmetric potential, we first present the approximate analytical solution of chirp-free FEA beam. Based on the analytical solution, we investigate analytically and numerically the split and collision of chirp-free FEA beam under diffraction modulation, and discuss the possibility of inverse design of diffraction modulation according to the predefined trajectory. Furthermore, through coherent combining technique, we derive the analytical solution of chirped FEA beam, and investigate analytically and numerically the asymmetric evolutions of chirped FEA beam in real space and spectral space, and discuss qualitatively the relation between the asymmetry and the chirp parameter. In the presence of PT-symmetric potential, we derive a general eigenvalue equation dependent on diffraction modulation and present the band structure modulated by varying fractional diffraction. Based on the band structure modulated by varying fractional diffraction, we study numerically the asymmetric conical

evolution of chirp-free FEA beam under diffraction modulation, which demonstrates that the propagation channels of FEA beam can be jointly manipulated by diffraction modulation and PT-symmetric potential. For chirped FEA beam, the competition effect between the chirp and the PT-symmetric potential on the beam dynamics is explored in detail.

Keywords Airy beam · Fractional Schrödinger equation · Diffraction modulation · PT-symmetric potential

1 Introduction

Airy wave packet is firstly observed by Berry and Balazs within the framework of quantum mechanics in 1979 [1]. It has been demonstrated that Airy wave packet has unique characteristics such as non-diffraction, self-acceleration and self-healing, but it is non-integrable and possesses infinite energy because of its oscillating tail [1]. In 1996, the finite energy Airy (FEA) wave packet with exponentially decaying tail is predicted in unbiased nonlinear photorefractive media [2], which manifests that the FEA wave packet can still maintain non-diffraction and self-acceleration over long distance. In 2007, one-dimension (1D) FEA beam is firstly explored and then observed experimentally in the context of optics [3, 4]. The

X. Bai · R. Yang (✉) · H. Jia · J. Bai
School of Physics and Electronics Engineering, Shanxi
University, Taiyuan 030006, China
e-mail: sxdxyrc@sxu.edu.cn

R. Yang
Collaborative Innovation Center of Extreme Optics,
Shanxi University, Taiyuan 030006, China

observation of 1D FEA beam in experiment provides the fundament to explore the dynamics of FEA beam in various conservative systems [5–7], such as in linear potential [5], parabolic potential [6] and on curved surfaces [7], etc. Importantly, based on the unique characteristics and physical realization, FEA beam is found various applications in particle manipulation [8], optical trapping [9], and curved plasma channel generation [10]. To achieve more applications, the propagation dynamics of Airy beam need to be precisely manipulated.

On the other hand, the fractional derivative included in fractional system, as an extension of integer-order derivative can be used to describe the real-world nonlocal dynamics of complex physical systems [11–13], such as the capacitor microphone [11], tumor-immune system [12] and permanent magnet synchronous motor system [13]. The fractional Schrödinger equation (FSE) is an extension of Schrödinger equation (SE) by constructing a fractional path integral over Lévy flight paths [14–16]. The FSE has successfully described the behavior of particles with fractional spin [17] and an effective model of Lévy crystal in condensed-matter environment [18], to name a few. Based on the mathematical analogy between the quantum mechanical SE and the paraxial equation of optical beam propagation, in 2015, Longhi inventively introduced the FSE into optics and proposed accessible optical implementation of fractional model in aspherical optical cavities [19]. Recently, Zhang et al. proposed that a honeycomb lattice can be a possible realization of the FSE by establishing a connection with the Dirac-Weyl equation [20]. So far, the propagation of beams governed by the FSE has also attracted wide research interest. Zhang et al. explored the propagation of Gaussian beam in FSE and demonstrated that the Gaussian beam may split into two non-diffracting sub-beams in the absence of external potential [21] and a parabolic potential can induce harmonic oscillation of Gaussian beam during propagation in FSE [22]. Nonlinear-wave structures in fractional system [23] governed by the FSE has also attracted wide research interest. Zeng et al. reported families of gap solitons with fractional diffraction and saturable nonlinearity [24]. Zang et al. and Xin et al. investigated the splitting dynamics of 1D and 2D Gaussian beams governed by linear variable-coefficient FSE, respectively [25, 26]. In addition, in linear and nonlinear regimes, the evolutions of other

beams, such as Bessel-Gaussian beam [27], necklace beam [28], soliton-like beam [29], Mainardi beam [30], Laguerre- Gaussian beam [31], Airy beam [32–36], have also been reported extensively. In view of the unique characteristics of Airy beam, Huang et al. studied the reflection and self-imaging of FEA beam induced by linear potential in FSE [32, 33]. Chen et al. investigated the dynamics and interaction of FEA beams in FSE with linear potential [34]. In addition, breather soliton forming [35] and autofocusing of Airy beam [36] are also hot topics. However, it is worth mentioning that most of the above reports on Airy beam are numerical. Because of the asymmetry and complex expression of Airy beam, the analytical Airy solution that theoretically describes its dynamics in FSE is difficult to derive. Up to now, the analytical solution of Airy beam in FSE with varying diffraction coefficient is still lacking, especially analytical chirped Airy solution.

As well known, non-Hermitian Hamiltonian may exhibit entirely real eigenvalue spectra provided it possesses PT-symmetry [37]. A Hamiltonian $\hat{H} = \hat{p}^2/2 + V(\hat{x})$ associated with a PT-symmetric potential indicates its commuting with the parity-time operator, i.e. $[\hat{H}, \hat{P}\hat{T}] = 0$, which implies $\hat{H}$ and $\hat{P}\hat{T}$ have the same eigenfunctions. Here the parity operator $\hat{P}$ is defined as $\hat{p} \rightarrow -\hat{p}, \hat{x} \rightarrow -\hat{x}$ and the time operator $\hat{T}$ as $\hat{p} \rightarrow -\hat{p}, \hat{x} \rightarrow \hat{x}, \hat{i} \rightarrow -\hat{i}$, where $\hat{p}$ and $\hat{x}$ represent the momentum and position operators, respectively. From this point, a necessary (but not sufficient) condition for a Hamiltonian to be PT-symmetric is $V(x) = V^*(-x)$, namely, whose real part is an even function of the position while imaginary part is odd of the position. Drawing an analogy to scalar paraxial optics, PT-symmetric potential can be realized by involving symmetric index guiding and antisymmetric gain/loss profile [38, 39]. In Optics, PT-symmetric potential plays an important role in the dynamics of beam. In conventional diffraction system, PT-symmetric potential can support double refraction and secondary emission of Gaussian beam [38, 39]. In fractional diffraction system, Zhang et al. and Wu et al. studied the propagation of Gaussian beam in PT-symmetric potential and found PT-symmetric potential can induce conical diffraction in linear regime [40, 41]. Also, in nonlinear regime with fractional diffraction in PT-symmetric potential, the existence and stability of various solitons [42–45] such as vortex

soliton [42], gap soliton [43] and oscillating soliton [44] and the symmetry-breaking of soliton [45] have drawn some attention. However, the diffraction behavior of Airy beam in modulated fractional diffraction system with PT-symmetric potential has not been explored. Indeed the manipulation of Airy beam in such varying fractional system is an unexploited practical issue that may be potential in regulating the dynamics of light beam and then used to fabricate optical devices.

In this work, we will investigate the evolution of FEA beam in fractional system with diffraction modulation and PT-symmetric potential. In the absence of PT-symmetric potential, we firstly derive the approximate analytical solutions of chirp-free FEA beam with diffraction modulation and discuss the inverse design of diffraction modulation according to the predefined trajectory. Furthermore, through coherent combining technique, we derive the analytical solution of chirped FEA beam in real space and spectral space and study qualitatively the relation between the asymmetry and the chirp parameter. In the presence of PT-symmetric potential, we present the band structure modulated by fractional diffraction based on a derived eigenvalue equation with diffraction modulation, and study numerically the asymmetric conical evolution of chirp-free FEA beam. Finally, for chirped FEA beam, we explore in detail the competition effect between the chirp and the PT-symmetric potential on the evolution of FEA beam.

The main structure of this work is as follows. In Sect. 2, the theoretical model is introduced, and the analytical and numerical results of chirp-free and chirped FEA beams in absence of PT-symmetric potential are presented in Sect. 3. In Sect. 4, a general eigenvalue equation with diffraction modulation is deduced and the band structure modulated by varying fractional diffraction is demonstrated and the evolution of chirp-free and chirped FEA beams in presence of PT-symmetric potential are studied numerically. In Sect. 5, we draw the conclusion from this work.

2 Theoretical model

The propagation of beams in fractional diffraction modulation system with PT-symmetric potential is governed by a variable coefficient FSE [25, 40]:

$$i\frac{\partial\Psi(x,z)}{\partial z} - \frac{1}{2}D(z)\left(-\frac{\partial^2}{\partial x^2}\right)^{\frac{\alpha}{2}}\Psi(x,z) + V(x)\Psi(x,z) = 0,$$
(1)

where $\Psi(x,z)$ is the complex envelope of beams, x and z are the normalized transverse coordinate and propagation distance, respectively. $\alpha(1 < \alpha \le 2)$ is the Lévy index, $D(z)$ denotes the diffraction modulation. $V(x)$ represents PT-symmetric potential in the form of $V(x) = V_0\left[\cos^2(x) + iW_0\sin(2x)\right]$ with the depth V_0 and the gain–loss coefficient W_0. For the limiting case $\alpha = 2$ and $D(z) = 1$, Eq. (1) degenerates to the usual SE that has been widely studied [38, 39]. To address the effects of fractional diffraction modulation and PT-symmetric potential on the evolution of FEA beam, we consider the opposite limiting case $\alpha = 1$ in the subsequent analysis.

3 In the absence of PT-symmetric potential

Firstly, we investigate the manipulation of FEA beam under fractional diffraction modulation in the absence of PT-symmetric potential, i.e. $V(x) = 0$. In this case, Eq. (1) is solvable for the limiting case $\alpha = 1$ through Fourier transform (FT). In inverse space, Eq. (1) can be written in the following form

$$i\frac{\partial\hat{\Psi}(k,z)}{\partial z} - \frac{1}{2}D(z)|k|\hat{\Psi}(k,z) = 0,$$
(2)

where $\hat{\Psi}(k,z)$ is the FT of $\Psi(x,z)$ and k is the spatial frequency. Equation (2) is a linear equation and possesses a general solution

$$\hat{\Psi}(k,z) = \hat{\Psi}(k,0)\exp\left[-\frac{i}{2}|k|\int_0^z D(\zeta)d\zeta\right],$$
(3)

where $\hat{\Psi}(k,0)$ is the FT of the initial beam $\Psi(x,0)$. Using inverse FT, one can give the analytical expression of the solution of Eq. (2)

$$\Psi(x,z) = \frac{1}{2\pi}\int_{-\infty}^{\infty}\hat{\Psi}(k,0)\exp\left[-\frac{i}{2}|k|\int_0^z D(\zeta)d\zeta\right]\exp(ikx)dk.$$
(4)

Thus, given an initial beam $\Psi(x,0)$, an analytical solution describing the evolution of the beam can be obtained. Zang et al. reported the explicit Gaussian

solution of Eq. (2) in Ref. [25], Zhang et al. presented Gaussian solution for the special case of constant coefficients of Eq. (2) in Ref. [21]. Until now, analytical solution of Airy beam for Eq. (2) with diffraction modulation has not been reported in the literature. Below we will try to seek the analytical solutions of FEA beam for Eq. (2) and to explore the interesting dynamics of the FEA beam in fractional diffraction modulation system. In the solving process of unique and complex Airy beam, some special treatments, such as reasonable assumption and approximation, combining technique [46], will be employed to deal with the asymmetry and cubical phase of FEA beam in real and inverse spaces.

3.1 Analytical solution of chirp-free FEA beam

Considering an initial chirp-free FEA beam

$$\Psi(x,0) = Ai(x)\exp(ax), \tag{5}$$

where $Ai(\bullet)$ is Airy function and $a(a>0)$ is the exponential apodization factor to ensure the containment of initial Airy tail [3–5]. For the sake of simplicity, in the subsequent analysis, we take $a = 0.1$ if not specified.

Substituting the FT of Eq. (5)

$$\hat{\Psi}(k,0) = \exp(-ak^2)\exp\left[\frac{i}{3}\left(k^3 - 3a^2k - ia^3\right)\right] \tag{6}$$

into Eq. (4), we obtain

$$\Psi(x,z) = \frac{1}{2\pi}\int_0^\infty \exp(-ak^2)\exp\left(\frac{a^3}{3}\right)$$
$$\exp\left[i\left(\frac{k^3}{3} - a^2k + kx\right)\right]\exp\left[-\frac{i}{2}k\int_0^z D(\zeta)d\zeta\right]dk$$
$$+ \frac{1}{2\pi}\int_{-\infty}^0 \exp(-ak^2)\exp\left(\frac{a^3}{3}\right)$$
$$\exp\left[i\left(\frac{k^3}{3} - a^2k + kx\right)\right]\exp\left[\frac{i}{2}k\int_0^z D(\zeta)d\zeta\right]dk. \tag{7}$$

Taking the assumption that $\int_0^z D(\zeta)d\zeta$ is negative for $k>0$ and positive for $k<0$, which is different from the ones in [21, 25], and applying the Euler's formula, Eq. (7) can be approximately written as

$$\Psi(x,z) \approx \frac{1}{4\pi}\int_{-\infty}^\infty \exp(-ak^2)\exp\left[\frac{i}{3}\left(k^3 - 3a^2k - ia^3\right)\right]$$
$$\exp\left\{ik\left[x - \frac{1}{2}\left|\int_0^z D(\zeta)d\zeta\right|\right]\right\}dk$$
$$+ \frac{1}{4\pi}\int_{-\infty}^\infty \exp(-ak^2)\exp\left[\frac{i}{3}\left(k^3 - 3a^2k - ia^3\right)\right]$$
$$\exp\left\{ik\left[x + \frac{1}{2}\left|\int_0^z D(\zeta)d\zeta\right|\right]\right\}dk. \tag{8}$$

Furthermore, employing the definitions of FT to Eq. (8), we can arrive at the analytical solution of chirp-free FEA beam of Eq. (2)

$$\Psi(x,z) \approx \frac{1}{2}Ai\left[x + \frac{1}{2}\int_0^z D(\zeta)d\zeta\right]\exp\left\{a\left[x + \frac{1}{2}\int_0^z D(\zeta)d\zeta\right]\right\}$$
$$+ \frac{1}{2}Ai\left[x - \frac{1}{2}\int_0^z D(\zeta)d\zeta\right]\exp\left\{a\left[x - \frac{1}{2}\int_0^z D(\zeta)d\zeta\right]\right\}. \tag{9}$$

It is obtained from Eq. (9) that the initial chirp-free FEA beam (5) evolves into two symmetric Airy-type sub-branches during propagation. The terms $\pm\frac{1}{2}\int_0^z D(\zeta)d\zeta$ in Eq. (9) describe the trajectories of the main lobes of two sub-branches, which suggest that the acceleration of Airy beam can be adjusted by the diffraction modulation $D(z)$. Figure 1 depicts the evolution of chirp-free FEA beam with $D(z) = d_1[1 + \xi\cos(\Omega z)]$, where d_1, ξ and Ω are the parameters of longitudinal diffraction modulation. In order to compare the dynamics of chirp-free FEA beam under $\alpha \neq 1$ and $\alpha = 1$, firstly, we present the amplitude evolution for $\alpha = 1.8, 1.5, 1.3, 1$ in Fig. 1a–d. Obviously, the chirp-free FEA beam is always accelerated and split regardless of the value of α. However, the smaller the α, the more evident the split, and the weaker the diffraction effect. It is clear to see that when $\alpha = 1$, the numerical evolution of the chirp-free FEA beam in Fig. 1d is in agreement with the analytical one in Fig. 1e that is plotted from Eq. (9). According to Eq. (9), it is easy to deduce that the main lobes of two sub-branches travel along the cosine trajectories $x = \pm\frac{d_1}{2}\left[z + \frac{\xi}{\Omega}\sin(\Omega z)\right]$, which is depicted by the green solid curves in Fig. 1d and e. It is noted that a collision of two sub-branches occurs and it is highly dependent on the diffraction modulation amplitude ξ. From the above trajectory expression, one can easily deduce that the two main lobes of sub-branches undergo a cross at $x = 0$, i.e.
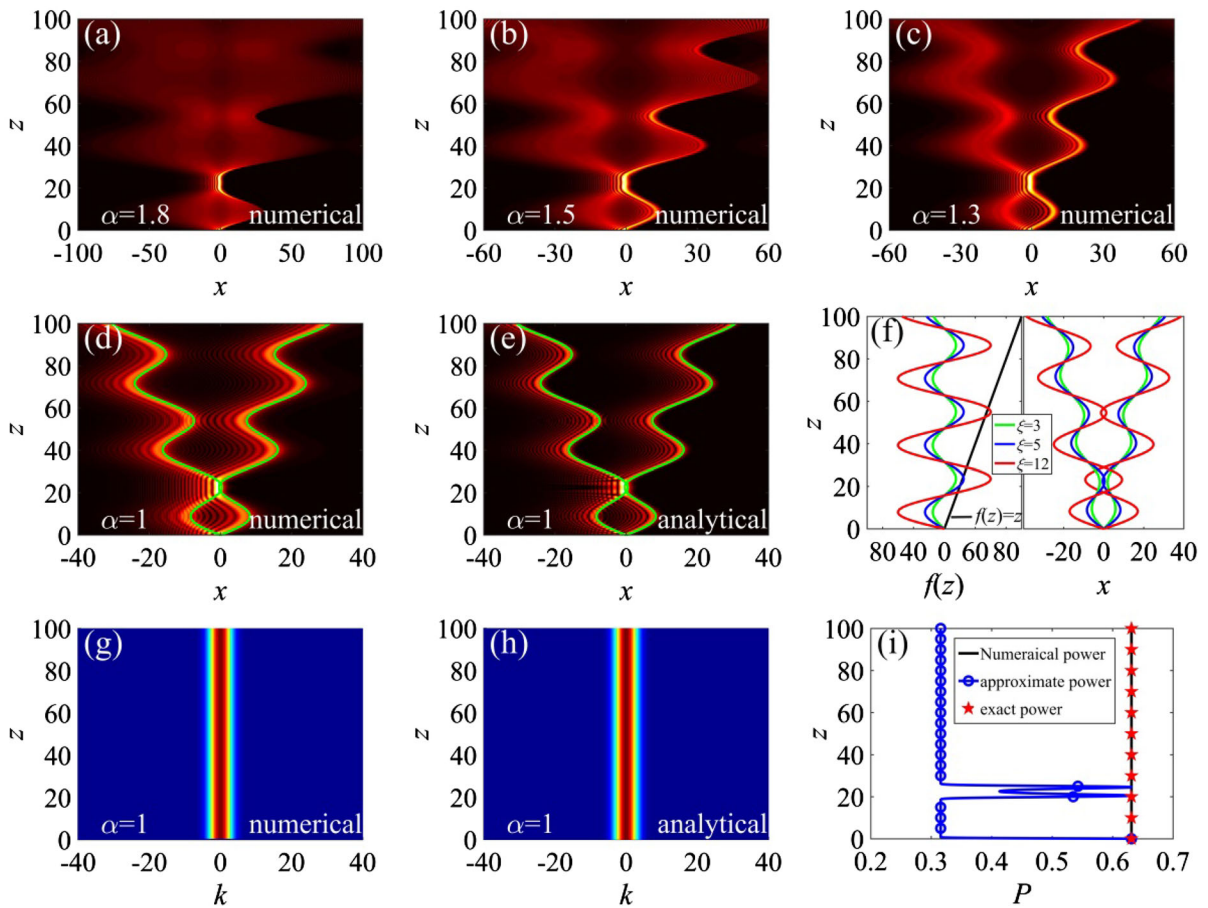
Fig. 1 Numerical evolutions **a** $\alpha = 1.8$, **b** $\alpha = 1.5$, **c** $\alpha = 1.3$, **d** $\alpha = 1$ and **e** analytical evolution (corresponding to **d**) of chirp-free FEA beam with diffraction modulation $D(z) = d_1[1 + \xi \cos(\Omega z)]$, where $d_1 = 0.5$, $\xi = 5$, $\Omega = 0.2$, and green solid curves show the trajectories of two main lobes;

f collision relation (the left) and trajectories (the right) of two main lobes for $\xi = 3, 5, 12$, black line marks $f(z) = z$; **g** and **h** Fourier spectra corresponding to **d** and **e**, respectively; **i** Power evolution. (Color figure online)

$z = -\frac{\xi}{\Omega} \sin(\Omega z)$. This implies a collision condition of $\max\left[-\frac{\xi}{\Omega} \sin(\Omega z)\right] \geq z$. In other words, when $\left|\frac{\xi}{\Omega}\right| \geq z$ at $z = nT + \frac{T}{4}$ for $\frac{\xi}{\Omega} < 0$ or $z = nT + \frac{3T}{4}$ for $\frac{\xi}{\Omega} > 0$ $\left(n = 0, 1, 2 \ldots, T = \frac{2\pi}{\Omega}\right)$, the collision occurs. Taking the example of $\frac{\xi}{\Omega} > 0$, only when $\xi \geq 2\left(n + \frac{3}{4}\right)\pi$, the collision of the two main lobes can occur, moreover, when $\frac{3}{2}\pi \leq \xi < \frac{7}{2}\pi$ $\left(\frac{7}{2}\pi \leq \xi < \frac{11}{2}\pi\right)$, one or two (three or four) cross-points are formed, as shown in the left of Fig. 1f. It is noted that in Fig. 1f, $f(z) = z$ (black solid line) and $f(z) = -\frac{\xi}{\Omega} \sin(\Omega z)$ (green, blue and red solid curves) depict the collision relation $z = -\frac{\xi}{\Omega} \sin(\Omega z)$. The collision trajectories of the two main lobes for different ξ are clearly illustrated in the right of Fig. 1f.

The controllable split and collision features of two main lobes may be useful in optical splitter and switch.

Different from the symmetric splitting propagation in real space shown in Fig. 1d and e, the chirp-free FEA beam follows an invariable spectrum evolution pattern in inverse space, as clearly displayed in Fig. 1g and 1h. In fact, this can be verified from Eqs. (3) and (6) that the Fourier amplitude spectrum of the chirp-free FEA beam during propagation is in a Gaussian form

$$\hat{\Psi}(k, z) = \exp(-ak^2) \exp\left(\frac{a^3}{3}\right) \exp\left\{i\left[\frac{k^3}{3} - a^2 k - \frac{1}{2}|k| \int_0^z D(\zeta) d\zeta\right]\right\}. \tag{10}$$

According to Eq. (10) and Parseval's theorem, the exact power of the beam can be described by

$$P_{exact} = \int_{-\infty}^{+\infty} |\Psi(x,z)|^2 dx = \frac{1}{2\pi} \int_{-\infty}^{+\infty} |\hat{\Psi}(k,z)|^2 dk$$
$$= \frac{1}{2\sqrt{2a\pi}} \exp\left(\frac{2a^3}{3}\right). \tag{11}$$

And the approximate power can be derived from Eqs. (8) and (9)

$$P_{approx} = \frac{1}{4\sqrt{2a\pi}} \exp\left(\frac{2a^3}{3}\right) \left\{1 + \exp\left[-\frac{1}{8a}\left(\int_0^z D(\zeta)d\zeta\right)^2\right]\right\}. \tag{12}$$

Figure 1i shows the comparison of the exact power (11), approximate power (12) and the numerical power by numerically solving Eq. (1) with $V(x) = 0$. It is observed from Fig. 1i that the numerical power remains unchanged and exhibits an excellent agreement with the exact power, but there is a deviation between the numerical power and the approximate one at the splitting regions of two sub-branches. This phenomenon can be explained by the difference in width between the numerical evolution and the analytical one in real space [25]. However, at the collision positions, the interaction of the sub-branches results in the recovery of approximate power to the initial level. This indicates that the FEA beam still maintains the characteristics of non-diffraction even though it is split into two colliding sub-Airy ones in fractional diffraction modulation system.

Based on the analytical expression of chirp-free Airy solution (9), an inverse problem can be solved through a reverse thinking [5]. Namely, one can design a diffraction modulation $D(z)$ through predefining the trajectories $x(z)$. In fact, in accordance with the trajectory expression $x(z) = \pm\frac{1}{2}\int_0^z D(\zeta)d\zeta$, the diffraction modulation $D(z)$ can be inversely engineered by the predefined trajectory $x(z)$,

$$D(z) = 2x'(z), \; x(0) = 0, \tag{13}$$

Typical trajectories of Airy beam may follow power, sinusoidal, hyperbolic laws, etc.[5]. We first consider a power law trajectory by assuming

$$x(z) = \pm[b(z - z_0)^c + b_0], \tag{14}$$

where b_0 is a constant to ensure $x(0) = 0$.

Substituting Eq. (14) into Eq. (13), it is easy to deduce that the diffraction modulation is in the form of $D(z) = 2bc(z - z_0)^{c-1}$. Figure 2a shows the evolution

of the chirp-free FEA beam modulated by power law fractional diffraction modulation. Figure 2b plots the velocity and acceleration of the main lobe of the right sub-branch under different power law fractional diffraction modulation. Figure 2c and d present the beam evolutions with two other typical trajectories in the forms of $x(z) = \pm\{2\text{arc } sin[\text{th}(z - 4)] + 2\text{arc } sin(\text{th } 4)\}$ and $x(z) = \pm\left[\sqrt{(z-4)^2 + 1} - 1\right]H(z-4)$, respectively, where $H(\bullet)$ denotes the Heaviside step function. The corresponding diffraction modulations take the forms of $D(z) = 4\text{sech}(z-4)$ and $D(z) = 2(z-4)H(z-4)\bigg/\sqrt{(z-4)^2 + 1}$, respectively. Therefore, one can engineer the fractional diffraction modulation system according to the predefined trajectories.

3.2 Coherent combining solution of chirped FEA beam

In practice, chirp plays an outstanding role in the compression, amplification and generation of short pulses in optical system. Along this line, a study of chirp in fractional system is very essential. In this section, we introduce an initial chirp to explore the effect on the dynamics of FEA beam in fractional system with varying diffraction.

For an initial chirped FEA beam

$$\Psi(x,0) = Ai(x)\exp(ax)\exp(i\beta x^2), \tag{15}$$

where β is the chirp parameter, we can theoretically obtain the chirped FEA solution of Eq. (2) by inserting the FT of Eq. (15) into Eq. (4)

$$\Psi(x,z) = \frac{1}{2\pi}\int_{-\infty}^{\infty}\sqrt{i\frac{\pi}{\beta}}Ai\left(\frac{k+ia}{2\beta} - \frac{1}{16\beta^2}\right)\exp\left(\frac{4a\beta k - a}{8\beta^2}\right)$$
$$\exp\left[-\frac{ik^2}{4\beta} + ik\left(\frac{1}{8\beta^2} + x\right) - \frac{i}{96\beta^3} + \frac{ia^2}{4\beta}\right]\exp\left[-\frac{i}{2}|k|\int_0^z D(\zeta)d\zeta\right]dk. \tag{16}$$

However, due to the asymmetry of Airy function and the complexity of the integral in Eq. (16), it is difficult to give explicit evolution expression of the chirped FEA beam. Up to now, the explicit solution of chirped FEA beam in fractional diffraction system has not been reported in literatures. We notice that the FEA beam can be composed by combining multiple off-axis coherent Gaussian beams [46], hence, in order
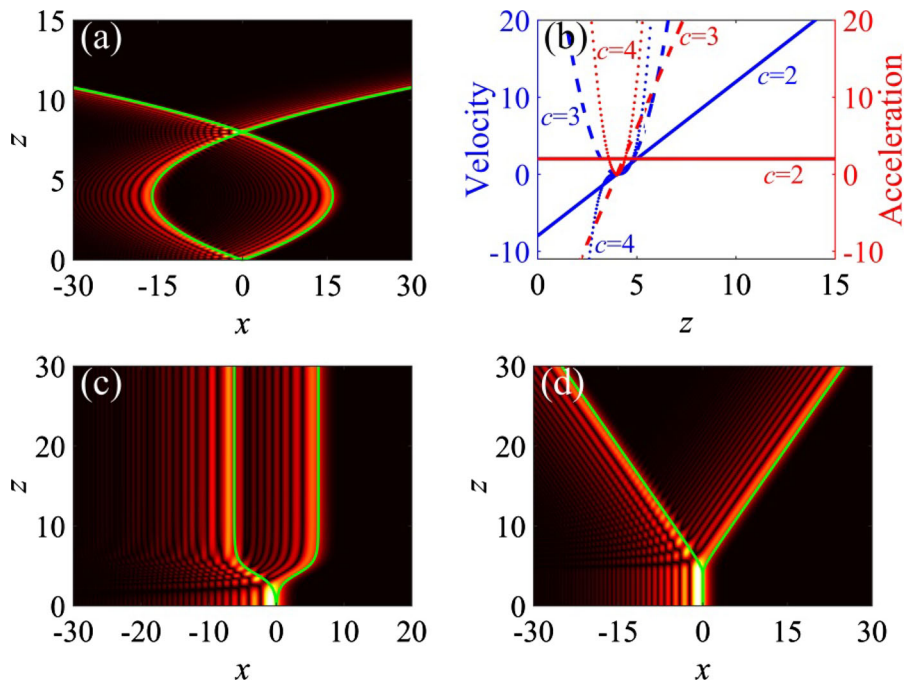
Fig. 2 Diffraction modulation of chirp-free FEA beams with predefined trajectories of **a** power law $x = \pm\left[(z-4)^2 - 16\right]$, **c** composite arcsine $x = \pm\{2\text{arc } sin[\text{th}(z-4)] + 2\text{arc } sin(\text{th } 4)\}$ and **d** piecewise $x = \pm\left[\sqrt{(z-4)^2 + 1} - 1\right] H(z-4)$; **b** is the velocity and acceleration of the right sub-branch of chirp-free FEA beam corresponding to **a** with different power law indexes. (Color figure online)

to obtain the explicit expression of chirped FEA solution, here we will employ the coherent combining technique to generate the initial chirped FEA beam,

$$\Psi(x,0) = \sum_{n=1}^{m} [\exp(i\pi)]^n A_n \exp\left[-\frac{(x-b_n)^2}{w_n^2}\right] \exp(i\beta x^2),$$

$$(17)$$

where A_n, b_n, w_n denote the amplitude, central position and waist width of the nth-order Gaussian beam, respectively. $[\exp(i\pi)]^n$ denotes the phase jump between the neighboring Gaussian beams. Exponential apodization of Airy beam can be achieved by fitting the parameters of A_n, b_n, w_n.

Figure 3 displays the curves of initial chirped FEA beams generated by the coherent combining technique and described by Eq. (15) with $a = 0.1$ and $\beta = 2$, where the inset is the fitting parameters A_n, b_n, w_n of
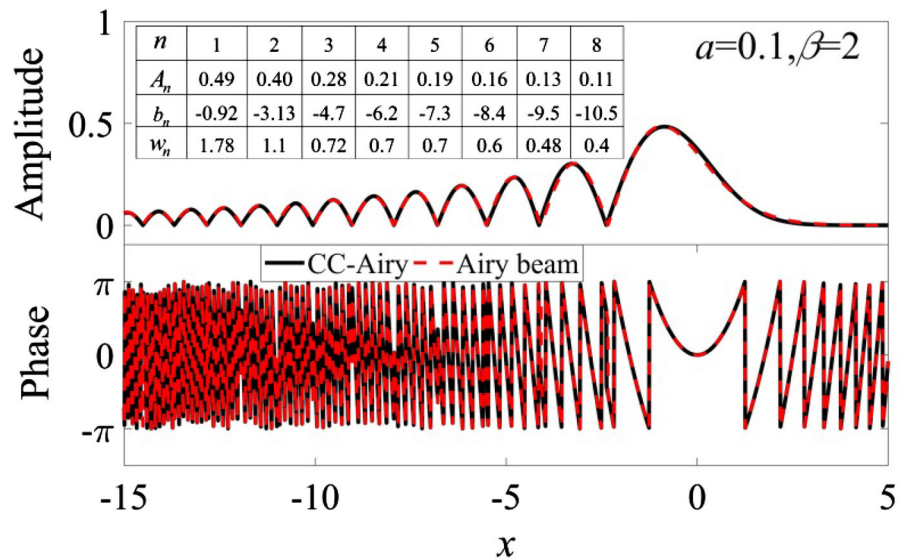
off-axis coherent Gaussian beams. Obviously, the amplitude and phase of the coherent combining Airy beam (CC-Airy beam) are well consistent with the one described by Eq. (15).

Taking the FT of initial CC-Airy beam with chirp (17)

$$\hat{\Psi}(k,0) = \sum_{n=1}^{m} [\exp(i\pi)]^n A_n w_n \sqrt{\frac{\pi}{1 - i\beta w_n^2}} \exp[ib_n(\beta b_n - k)]$$
$$\exp\left[-\frac{w_n^2(2\beta b_n - k)^2}{4(1 - i\beta w_n^2)}\right],$$

$$(18)$$

and substituting it into Eq. (4), the coherent combining solution of the chirped CC-Airy beam of Eq. (2) can be written as

Fig. 3 Comparison of the
initial CC-Airy beam and
the initial chirped Airy beam
(15) with $a = 0.1$, $\beta = 2$.
Inset table is the fitting
parameters A_n, b_n, w_n, of
off-axis coherent Gaussian
beams for the CC-Airy
beam. (Color figure online)

n	1	2	3	4	5	6	7	8
A_n	0.49	0.40	0.28	0.21	0.19	0.16	0.13	0.11
b_n	-0.92	-3.13	-4.7	-6.2	-7.3	-8.4	-9.5	-10.5
w_n	1.78	1.1	0.72	0.7	0.7	0.6	0.48	0.4

$$\Psi(x,z) = \begin{cases} \sum_{n=1}^{m} [\exp(i\pi)]^n A_n \exp\left\{ i\beta b_n \left[2x + \int_0^z D(\zeta)d\zeta - b_n \right] \right\} \\ \exp\left\{ -\frac{1 - i\beta w_n^2}{w_n^2} \left[x + \frac{1}{2} \int_0^z D(\zeta)d\zeta - b_n \right]^2 \right\} + h_+(x,z), \ \beta > 0 \\ \sum_{n=1}^{m} [\exp(i\pi)]^n A_n \exp\left\{ i\beta b_n \left[2x - \int_0^z D(\zeta)d\zeta - b_n \right] \right\} \\ \exp\left\{ -\frac{1 - i\beta w_n^2}{w_n^2} \left[x - \frac{1}{2} \int_0^z D(\zeta)d\zeta - b_n \right]^2 \right\} + h_-(x,z), \ \beta < 0 \end{cases},$$

(19)

where

$$h_\pm(x,z) = \pm \sum_{n=1}^{m} [\exp(i\pi)]^n \frac{A_n w_n}{2\sqrt{\pi(1 - i\beta w_n^2)}}$$

$$\exp\left\{ i\beta b_n \left[2x - \int_0^z D(\zeta)d\zeta - b_n \right] \right\} \int_{|2\beta b_n|}^{+\infty}$$

$$\exp\left\{ \pm ik \left[x - \frac{1}{2} \int_0^z D(\zeta)d\zeta - b_n \right] \right\} \exp\left[-\frac{w_n^2 k^2}{4(1 - i\beta w_n^2)} \right] dk$$

$$\mp \sum_{n=1}^{m} [\exp(i\pi)]^n \frac{A_n w_n}{2\sqrt{\pi(1 - i\beta w_n^2)}}$$

$$\exp\left\{ i\beta b_n \left[2x + \int_0^z D(\zeta)d\zeta - b_n \right] \right\} \int_{|2\beta b_n|}^{+\infty}$$

$$\exp\left\{ \pm ik \left[x + \frac{1}{2} \int_0^z D(\zeta)d\zeta - b_n \right] \right\} \exp\left[-\frac{w_n^2 k^2}{4(1 - i\beta w_n^2)} \right] dk$$

(20)

with

$$|h_\pm(x,z)| \le \sum_{n=1}^{m} \frac{A_n w_n}{\sqrt{\pi}} \left(\frac{1}{1 + \beta^2 w_n^4} \right)^{\frac{1}{4}} \int_{|2\beta b_n|}^{+\infty}$$

$$\exp\left[-\frac{w_n^2 k^2}{4(1 + \beta^2 w_n^4)} \right] dk = \sum_{n=1}^{m} A_n \left(1 + \beta^2 w_n^4 \right)^{\frac{1}{4}} erfc$$

$$\left(\frac{|\beta b_n| w_n}{\sqrt{1 + \beta^2 w_n^4}} \right),$$

(21)

in which $erfc(\bullet)$ denotes the complementary error function.

It should be pointed out that in Eq. (20), $h_\pm(x,z)$ is non-neglectable due to the restraint between the lower limit $|2\beta b_n|$ of integral and the integrand term $\exp\left[-w_n^2 k^2 / 4(1 - i\beta w_n^2) \right]$. As a consequence, the chirped CC-Airy beam will evolve into two asymmetric sub-branches no matter what the value of the chirp parameter, which is quite different from the results for linear chirp in Refs. [21, 25]. Figure 4a1, a2 and b1, b2 depict the analytical evolution governed by Eqs. (19) and (20) and the directly numerical simulations of the initial chirped FEA beam (15). From the analytical and numerical results, it is clearly seen that the chirped FEA beam splits into two sub-branches with different intensities, moreover, the positive chirp leads to a suppression of the right sub-branch [see Fig. 4a1, b1], while the negative chirp gives rise to a suppression of the left sub-branch [see Fig. 4a2, b2]. Also, the
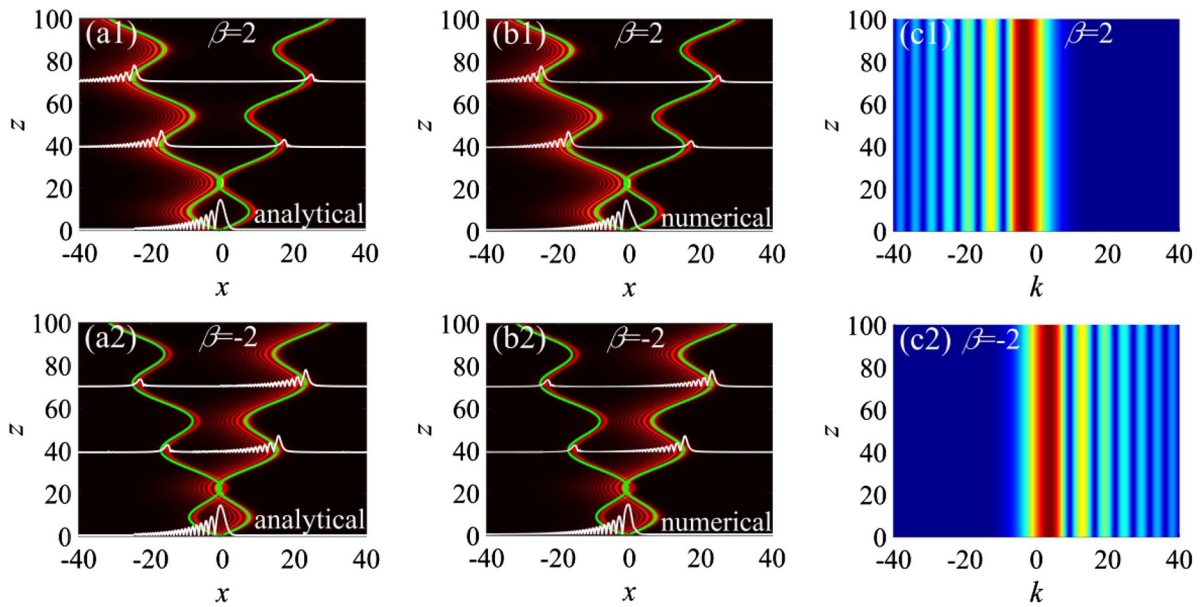
Fig. 4 Evolution of the chirped FEA beam: **a1** and **a2** analytical CC-Airy beam, **b1** and **b2** the corresponding numerical results; **c1** and **c2** the Fourier spectra in inverse space. In **a1**, **b1** and **a2**, **b2**, the green curves show the trajectories of two main lobes, and the white curves plot the beam amplitudes at $z = 0$, 40, and 70. (Color figure online)

amplitude profiles at typical distances of $z = 0$, 40 and 70 verify our analytical and numerical findings, which are depicted by the white solid curves in Fig. 4a and b. Interestingly, this asymmetric split in real space leads to an Airy-like Fourier spectrum in inverse space over the propagation, as shown in Figs. 4c1 and c2, which are quite different from the chirp-free ones shown in Fig. 1d and e.

In fact, the asymmetry of two sub-branches resulted from the initial chirp can be explained qualitatively by the $h_{\pm}(x, z)$ in Eq. (19). The maximum of $|h_{\pm}(x, z)|$ can be estimated as

$$\max(|h_{\pm}(x, z)|) = \sum_{n=1}^{m} A_n \left(1 + \beta^2 w_n^4\right)^{\frac{1}{4}} erfc\left(\frac{|\beta b_n| w_n}{\sqrt{1 + \beta^2 w_n^4}}\right).$$
(22)

Combining Eq. (22) with Eqs. (19) and (20), one can deduce that $h_{\pm}(x, z)$ in (19) and (20) plays a key role in the asymmetric evolution of the chirped CC-Airy beam. The relationship of the $\max(|h_{\pm}(x, z)|)$ and the chirp parameter β is plotted in Fig. 5a. With the increasing of $|\beta|$, $\max(|h_{\pm}(x, z)|)$ rapidly deceases to a minimum critical value at certain $|\beta|$ [see points 'B'
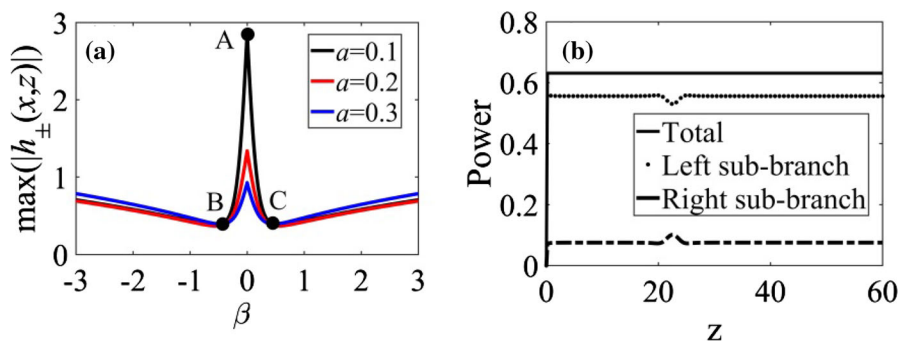
Fig. 5 **a** The relationship of $\max(|h_{\pm}(x, z)|)$ and β for different apodization factor a. The points 'A', 'B' and 'C' respectively correspond to $\beta = 0$, -0.47, 0.47; **b** power evolution of the positive chirped Airy beam. (Color figure online)

and 'C' in Fig. 5a], and then slowly increases. Moreover, by analyzing the expressions of Eqs. (19) and (20), it is found that the larger the $\max(|h_\pm(x,z)|)$, the more comparable the two sub-branches of the chirped CC-Airy solution (19). Hence, at point 'A', i.e. $\beta = 0$, the sub-branches are symmetric, which corresponds to the chirp-free case in Fig. 1, while at points 'B' and 'C' where $\max(|h_\pm(x,z)|)$ is minimum at $|\beta| = 0.47$, the first term in the solution (19) will dominate the evolution of the chirped CC-Airy beam, which gives rise to more asymmetry of two sub-branches. Furthermore, it is found from Fig. 5a that the critical values at points 'B' and 'C' are almost same, i.e.,$|\beta| = 0.47$ for different apodization factor a. In addition, the power evolution of the positive chirped Airy beam is shown in Fig. 5b. It is clear to see that the total power is conserved, while the power of two sub-branches is apparently asymmetric, accompanying with an energy exchange at the collision position.

4 In the presence of PT- symmetric potential

In the presence of PT-symmetric potential, when the FEA beam propagates in the fractional system (1) with diffraction modulation, Eq. (1) is non-integrable and has no analytical Airy solution. Therefore, we will study numerically the innovative characteristics arising from the interaction between the modulated fractional diffraction and the PT-symmetric potential, which will be demonstrated as below.

4.1 Band structure

Due to the diffraction modulation in Eq. (1), the band spectrum for the periodic PT-symmetric potential is the function of z and k. Hence we assume the stationary solution of Eq. (1) is of the form $\phi_n(x,k)\exp[i\mu_n(k,z)\,z]$, where $\phi_n(x,k)$ represents the Bloch mode and $\mu_n(k,z)$ is the propagation constant. According to the Floquet-Bloch theorem [47], $\phi_n(x,k)$ can be assumed as $\phi_n(x,k) = q_k(x)\exp(ikx)$ with $q_k(x) = q_k(x + D)$, where D is the period of the PT-symmetric potential. Using plane-wave expansion method,$q_k(x)$and $V(x)$can be written as $\quad q_k(x) = \sum\limits_n B_n \exp(iK_n x)$and $\quad V(x) = \sum\limits_m C_m \exp(iK_m x)$, respectively, where $K_j = 2\pi j/D(j = n,\ m)$

and $C_m = \frac{1}{D}\int_D V(x)\exp(-iK_m x)dx$. Substituting these expressions into Eq. (1) with $\alpha = 1$ and multiplying with $\exp[-i(k + K_q)x]$, and then taking the integral over $x \in (-\infty,\ \infty)$, one can derive the eigenvalue problem

$$-\frac{1}{2}D(z)|k + K_q|B_q + \sum_m C_m B_{q-m} = (\mu + z\mu_z')B_q.$$
(23)

It is noted that Eq. (23) represents a general eigenvalue problem dependent on the diffraction modulation, and importantly, the eigenvalue equation can be applied to investigate the band structure of any varying fractional systems with periodic potential. By numerically solving Eq. (23), the band structure of the system (1) can be obtained. Figure 6 depicts the band structures for the periodic PT-symmetric potential when $D(z) = d_1[1 + \xi\cos(\Omega z)]$. Clearly, the band spectra are highly dependent on the diffraction modulation $D(z)$, which is different from the previous reports in Refs. [38–41]. It can be seen from Fig. 6 that the band spectra are periodically modulated along the propagation distance z due to the periodic diffraction modulation, however, the band spectra still remain the substantive characteristics at a certain propagation distance. To be specific, below the PT threshold $W_0^{th} = 0.5$, the band spectrum is entirely real and all the forbidden gaps are open, as shown in Fig. 6a; at the threshold, the first two bands merge at the edges of the Brillouin zone and the first band gap closes, which is described in Fig. 6b; above the threshold, as shown Fig. 6c and d, the spontaneous symmetry breaking occurs, as a result, the band spectrum is complex with an oval-like double-valued band structure in real parts. It is noted that at a certain propagation distance, the band structure near the center of the Brillouin zone is linear, which will result in a constant group velocity and a conical spread in the fractional system with PT-symmetric potential [40, 41].
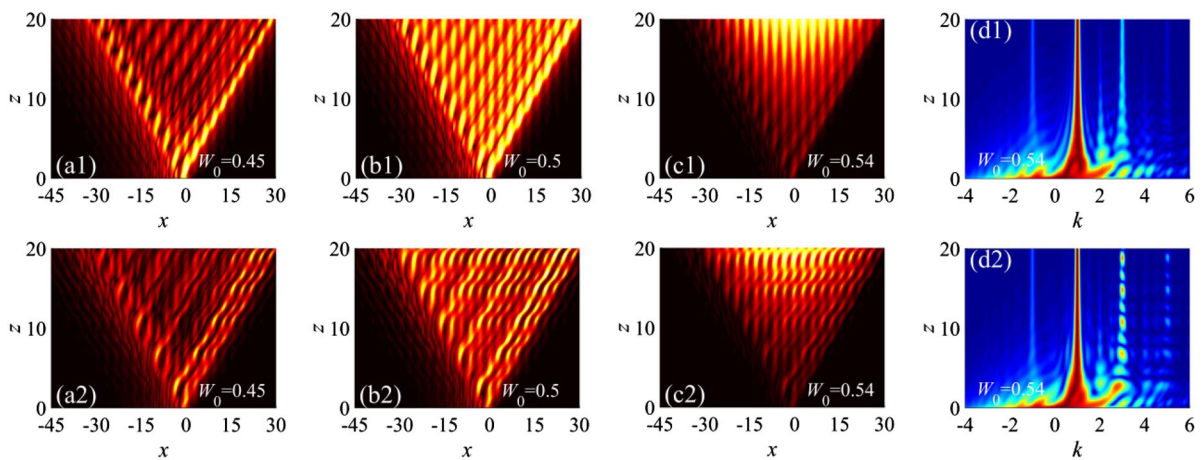
4.2 Chirp-free FEA beam

In the PT-symmetric system (1) with fractional diffraction modulation, unique characteristics of Airy beam and fractional diffraction modulation will result in some novel and interesting phenomena, which are quite different from the dynamics of Gaussian beam in usual PT-symmetric system [38, 39] and the PT-
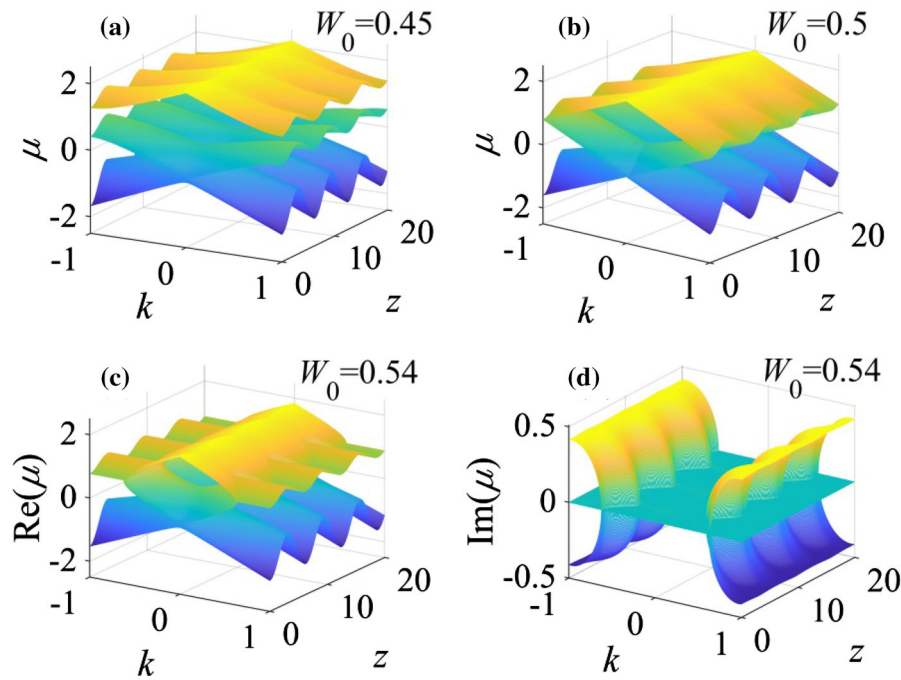
Fig. 6 Band structures governed by Eq. (23) with $D(z) = d_1[1 + \xi \cos(\Omega z)]$ for **a** $W_0 = 0.45$, **b** $W_0 = 0.5$, **c** and **d** $W_0 = 0.54$. Other parameters: $d_1 = 2, \xi = 0.2, \Omega = 1$. (Color figure online)

symmetric system with fractional constant coefficient diffraction [40, 41]. Figure 7 depicts the evolution of chirp-free FEA beam in the PT-symmetric system with fractional diffraction modulation $D(z) = d_1[1 + \xi \cos(\Omega z)]$. For weak diffraction modulation, i.e. $\xi \ll 1$, the PT-symmetric potential plays a dominant role in the evolution of chirp-free FEA

beam, as shown in Fig. 7a1-c1, in which it can be seen that the beam evolves in an asymmetrical conical form. Also, it is observed from Fig. 7a1 and b1 that the beam possesses more energy at the PT threshold than that below the threshold, while its power is asymmetrically and drastically amplified above the threshold as a result of the complex band spectrum after PT

Fig. 7 Evolution of chirp-free FEA beam in the periodic PT-symmetric system with fractional diffraction modulation. Top row ($\xi = 0.01$) and bottom row ($\xi = 0.4$): **a1, a2** $W_0 = 0.45$;

b1, b2 $W_0 = 0.5$; **c1, c2** $W_0 = 0.54$; **d1** and **d2** normalized Fourier spectra corresponding to **c1** and **c2**, respectively. Other parameters: $V_0 = 2, d_1 = 3, \Omega = 0.5\pi$. (Color figure online)

symmetry breaking, as plotted in Fig. 7c1. Moreover, some interference fringes appear near the left edge of conical evolution due to the oscillating tails of Airy beam, and the energy at the right edge of conical evolution is stronger than that at the left edge because main lobe of Airy beam possesses larger intensity. The above two features arising from unique characteristics of Airy beam are markedly different from the symmetric conical diffraction of Gaussian beam [40, 41]. For strong diffraction modulation, the chirp-free FEA beam conically evolves along unidirectional bend channels below and at the PT threshold, while above the PT threshold, the rapidly amplified chirp-free FEA beam diffracts conically along the modulated straight channels, as shown in Fig. 7a2-c2.

In order to deeply understand the evolution of FEA beam in PT-symmetric system with fractional diffraction modulation, we further discuss the Fourier spectrum in inverse space by taking the FT of Eq. (1) with $\alpha = 1$

$$
\begin{aligned}
&i\frac{\partial \hat{\Psi}(k,z)}{\partial z} + \frac{1}{2}[V_0 - |k|D(z)]\hat{\Psi}(k,z) \\
&+ \frac{V_0}{2}(0.5 - W_0)\hat{\Psi}(k+2,z) \\
&+ \frac{V_0}{2}(0.5 + W_0)\hat{\Psi}(k-2,z) \\
&= 0.
\end{aligned} \tag{24}
$$

Obviously, the Fourier spectrum in Eq. (24) is discrete in the periodic PT-symmetric potential and the discrete spectra occur coupling at $k + 2$, k and $k - 2$ during propagation [40]. Figure 7d1 and d2 plot the spectra evolution of chirp-free FEA beam for the case above the PT threshold under weak and strong diffraction modulations, respectively. It is clear to see that for both weak and strong modulations, at the beginning of propagation, the spectra are wide and there is much interference between different k because the Fourier spectrum (6) of chirp-free FEA beam is in a wide Gaussian form. Moreover, the discrete coupling spectra appear increased intensity at k and $k - 2$, which can be explained by Eq. (24). For a given V_0, above the PT threshold, i.e. $W_0 > 0.5$, the magnitude of discrete spectrum is larger at $k - 2$ than that at $k + 2$, resulting in that the spectral coupling at k and $k - 2$ is dominant during propagation. Compared Fig. 7d1 with d2, it is noted that for strong diffraction modulation the dominated spectrum components appear periodic features [see Fig. 7d2], which arises from that the discrete spectrum coefficient is dependent on the diffraction modulation $D(z)$.
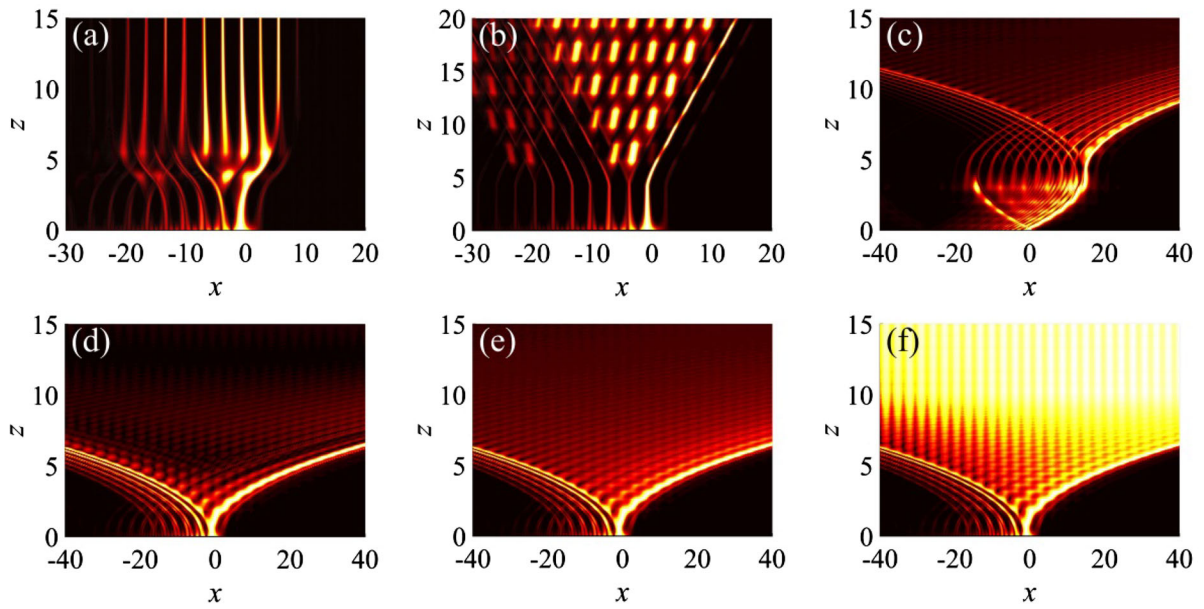
4.3 Chirped FEA beam

In Sect. 3, we demonstrated analytically and numerically the effect of chirp on the evolution of FEA beam in the system (1) without PT-symmetric potential. Here we emphasize the competition effect of the chirp and the PT-symmetric potential on the evolution of FEA beam at the PT threshold under the fractional diffraction modulation $D(z) = d_1[1 + \xi\cos(\Omega z)]$, as shown in Fig. 8. By comparing Fig. 8a and b, it is clearly seen that the smaller depth V_0 of PT-symmetric potential induces the weaker conical diffraction effect; while positive initial chirp results in energy mainly flowing to the left edge of the conical evolution. As the depth V_0 is increased, the conical diffraction effect is obviously enhanced, accompanying with similar diffraction fringes with that in Fig. 7b2. Different from Fig. 7b2, the positive initial chirp yields an enhanced interference at left edge between the conical diffraction fringes and the tail interference fringes, as shown in Fig. 8a and b. From Fig. 8c and d, it can be observed that negative initial chirp gives rise to strong interference fringes near the right edge of the conical evolution. Moreover, the increased depth V_0 reinforces the conical diffraction fringes. It is noteworthy
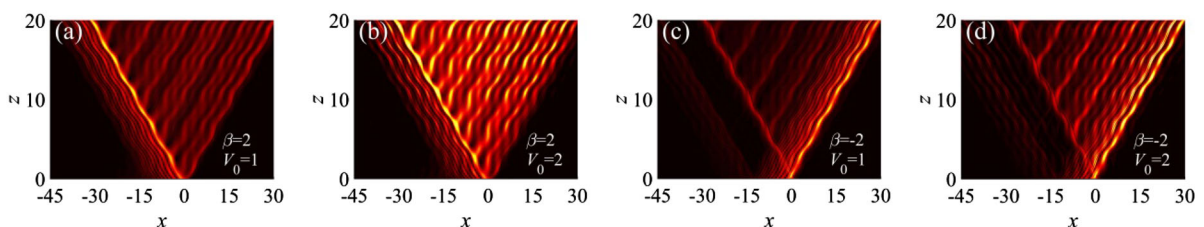
Fig. 8 Evolution of chirped FEA beam at the PT threshold: **a** $\beta = 2$, $V_0 = 1$; **b** $\beta = 2$, $V_0 = 2$; **c** $\beta = -2$, $V_0 = 1$; **d** $\beta = -2$, $V_0 = 2$. Other parameters: $d_1 = 3$, $\xi = 0.4$, $\Omega = 0.5\pi$. (Color figure online)

Fig. 9 Top row: evolution of chirped FEA beams under typical diffraction modulations in PT-symmetric system: **a** $D(z) = 4\mathrm{sech}(z - z_0)$; **b** $D(z) = 2(z - z_0)H(z - z_0)$ $\Big/ \sqrt{(z - z_0)^2 + 1}$; **c** $D(z) = 4(z - z_0)$ with $z_0 = 4$. Bottom row: evolution of chirped FEA beams under different gain/loss coefficients W_0: **d** $W_0 = 0.45$; **e** $W_0 = 0.5$; **f** $W_0 = 0.54$ for $D(z) = 4(z - z_0)$ with $z_0 = 0$. Other parameters: $V_0 = 4, \beta = 2$. (Color figure online)

that the competition between the negative chirp and the PT-symmetric potential will hardly influence the tail interference fringes at the left of the conical evolution, which is different from the case with positive chirp in Fig. 8a and b. This difference can be attributed to the inherent asymmetry of Airy beam.

4.4 With different diffraction modulations

Finally, we discuss the evolution of chirped FEA beam in PT-symmetric system (1) with different fractional diffraction modulations. Figure 9a-c show the normalized evolution of chirped FEA beam at the PT threshold under three typical diffraction modulations ①$D(z) = 4\mathrm{sech}(z - z_0)$, ②$D(z) = 2(z - z_0)H(z - z_0)$ $\Big/ \sqrt{(z - z_0)^2 + 1}$, in which $H(\bullet)$ denotes the Heaviside step function, ③$D(z) = 4(z - z_0)$ [5]. It is obvious to see that hyperbolic secant, Heaviside step and linear diffraction modulations can induce straight, discrete conical and parabolic channels of propagation, respectively after a distance of z_0. Therefore, one can manipulate the propagation channels of FEA beam along the desired paths by choosing diffraction modulation. It should be pointed that the designed

propagation channels are also related to the gain/loss coefficient W_0 of PT-symmetric potential. Figure 9d-f present the normalized evolution of chirped FEA beam for $D(z) = 4(z - z_0)$ with $z_0 = 0$ under different W_0. It can be deduced by comparing Fig. 9d-f that the gain/loss coefficient W_0 affects the energy distribution of the beam at the interference channels.

5 Conclusion

In conclusion, we have studied the evolution of FEA beam in fractional system with diffraction modulation and PT-symmetric potential. In the absence of PT-symmetric potential, firstly, we presented the approximate analytical solution of chirp-free FEA beam. Based on the analytical solution, we investigated analytically and numerically the split and collision of chirp-free FEA beam under diffraction modulation, and discussed the possibility of inverse design of diffraction modulation according to the predefined trajectory. It is found that the chirp-free FEA beam splits into two symmetric sub-branches during propagation and the collision of two sub-branches highly depends on the amplitude of diffraction modulation.

Furthermore, through coherent combining technique, we derived the analytical solution of chirped FEA beam, and investigated analytically and numerically the asymmetric evolution of chirped FEA beam in real space and spectral space, and discussed qualitatively the relation between the asymmetry and the chirp parameter. The results show that the chirp dominates the asymmetry of two sub-branches. In the presence of PT-symmetric potential, we investigated the band structure modulated by varying fractional diffraction based on a derived eigenvalue equation with diffraction modulation, and then studied numerically the asymmetric conical evolution of chirp-free FEA beam in the PT-symmetric system with weak and strong diffraction modulations. It is found that under strong diffraction modulation, the chirp-free FEA beam asymmetrically evolves along unidirectional bend channels below and at the PT threshold, while above the PT threshold, the FEA beam is rapidly amplified and diffracts conically along the modulated straight channels. For chirped FEA beam, the competition effect between the chirp and the PT-symmetric potential on the beam evolution is explored in details. This work provides a method for inverse design of the fractional diffraction modulation system and the presented results are potential in the fabrication of optical splitter and switch.

Data availability Our manuscript has no associated data.

Declarations

Competing interest The authors have no relevant financial or non-financial interests to disclose.

References

1. Berry, M.V., Balazs, N.L.: Nonspreadingwave packets. Am. J. Phys. **47**(3), 264 (1979)

2. Christodoulides, D.N., Coskun, T.H.: Diffraction-free planar beams in unbiased photorefractive media. Opt. Lett. **21**(18), 1460 (1996)

3. Siviloglou, G.A., Christodoulides, D.N.: Accelerating finite energy airy beams. Opt. Lett. **32**(8), 979–981 (2007)

4. Siviloglou, G., Broky, J., Dogariu, A., Christodoulides, D.N.: Observation of accelerating Airy beams. Phys. Rev. Lett. **99**(21), 213901 (2007)

5. Efremidis, N.K.: Airy trajectory engineering in dynamic linear index potentials. Opt. Lett. **36**(15), 3006–3008 (2011)

6. Zhang, Y.Q., Belic, M.R., Zhang, L., Zhong, W.P., Zhu, D.Y., Wang, R.M., Zhang, Y.P.: Periodic inversion and phase transition of fnite energy Airy beams in a medium with parabolic potential. Opt. Express **23**(8), 10467–10480 (2015)

7. Tian, K., Wang, Z.Y.: Propagation properties of finite Airy beams on curved surfaces. Opt. Express **30**(4), 5274–5282 (2022)

8. Baumgartl, J., Mazilu, M., Dholakia, K.: Optically mediated particle clearing using Airy wavepackets. Nat. Photonic **2**(11), 675–678 (2008)

9. Zhang, P., Prakash, J., Zhang, Z., Mills, M.S., Efremidis, N.K., Christodoulides, D.N., Chen, Z.: Trapping and guiding microparticles with morphing autofocusing Airy beams. Opt. Lett. **36**(15), 2883–2885 (2011)

10. Polynkin, P., Kolesik, M., Moloney, J.V., Siviloglou, G.A., Christodoulides, D.N.: Curved plasma channel generation using ultraintense Airy beams. Science **324**(5924), 229–232 (2009)

11. Jajarmi, A., Baleanu, D., Vahid, K.Z., Pirouz, M.H., Asad, J.H.: A new and general fractional Lagrangian approach: a capacitor microphone case study. Result Phys. **31**, 104950 (2021)

12. Jajarmi, A., Baleanu, D., Vahid, K.Z., Mobayen, S.: A general fractional formulation and tracking control for immunogenic tumor dynamics. Math. Meth. Appl. Sci. **45**(2), 667–680 (2022)

13. Zhang, S.H., Wang, C., Zhang, H.L., Ma, P., Li, X.K.: Dynamic analysis and bursting oscillation control of fractional-order permanent magnet synchronous motor system. Chaos Soliton Fract. **156**, 111809 (2022)

14. Laskin, N.: Fractional quantum mechanics and Lévy path integrals. Phys. Lett. A **268**(4–6), 298–305 (2000)

15. Laskin, N.: Fractional quantum mechanics. Phys. Rev. E **62**(3), 3135–3145 (2000)

16. Laskin, N.: Fractional Schrödinger equation. Phys. Rev. E **66**(5), 056108 (2002)

17. Herrmann, R.: Fractional Calculus: an Introduction for Physicists. World Scientific, Singapore (2011)

18. Stickler, B.A.: Potential condensed-matter realization of space-fractional quantum mechanics: the one-dimensional Lévy crystal. Phys. Rev. E **88**(1), 012120 (2013)

19. Longhi, S.: Fractional Schrödinger equation in optics. Opt. Lett. **40**(6), 1117–1120 (2015)

20. Zhang, D., Zhang, Y.Q., Zhang, Z.Y., Ahmed, N., Zhang, Y.P., Li, F.L., Belić, M.R., Xiao, M.: Unveiling the link between fractional Schrödinger equation and light propagation in honeycomb lattice. Ann. Phys. (Berlin) **529**(9), 1700149 (2017)

21. Zhang, Y.Q., Zhong, H., Belić, M.R., Ahmed, N., Zhang, Y.P., Xiao, M.: Diffraction-free beams in fractional Schrödinger equation. Sci. Rep. **6**, 23645 (2016)
22. Zhang, Y.Q., Liu, X., Belić, M.R., Zhong, W.P., Zhang, Y.P., Xiao, M.: Propagation dynamics of a light beam in a fractional Schrödinger equation. Phys. Rev. Lett. **115**(18), 180403 (2015)
23. Mihalache, D.: Localized structures in optical and matter-wave media: a selection of recent studies. Rom. Rep. Phys. **73**(2), 403 (2021)
24. Zeng, L.W., Belić, M.R., Mihalache, D., Shi, J.C., Li, J.W., Li, S.Q., Lu, X.W., Cai, Y., Li, J.Z.: Families of gap solitons and their complexes in media with saturable nonlinearity and fractional diffraction. Nonlinear Dyn. **108**(2), 1671–1680 (2022)
25. Zang, F., Wang, Y., Li, L.: Dynamics of Gaussian beam modeled by fractional Schrödinger equation with a variable coefficient. Opt. Express **26**(18), 23740–23750 (2018)
26. Xin, W., Song, L.J., Li, L.: Propagation of Gaussian beam based on two-dimensional fractional Schrödinger equation. Opt. Commun. **480**, 126483 (2021)
27. Zhang, Y.G., Wu, Z.K., Ru, J.M., Wen, F., Gu, Y.Z.: Evolution of the Bessel-Gaussian beam modeled by the fractional Schrödinger equation. J. Opt. Soc. Am. B **37**(11), 3414–3421 (2020)
28. Dong, L.W., Liu, D.S., Qi, W., Wang, L.X., Zhou, H., Peng, P., Huang, C.M.: Necklace beams carrying fractional angular momentum in fractional systems with a saturable nonlinearity. Commun. Nonlinear Sci. Numer. Simul. **99**, 105840 (2021)
29. Wang, J.F., Jin, Y., Gong, X.G., Yang, L.Z., Chen, J., Xue, P.P.: Generation of random soliton-like beams in a nonlinear fractional Schrödinger equation. Opt. Express **30**(5), 8199–8211 (2022)
30. Habibi, F., Moradi, M.: Comparison of Mainardi, cos-Mainardi and cosh-Mainardi beams with and without optical vortex in FT and FrFT systems. Phys. Scr. **97**(4), 045406 (2022)
31. Zhou, W.J., Liu, A.X., Huang, X.W., Bai, Y.F., Fu, X.Q.: Propagation dynamics of Laguerre-Gaussian beams in the fractional Schrödinger equation with noise disturbance. J. Opt. Soc. Am. A **39**(4), 736–743 (2022)
32. Huang, X.W., Shi, X.H., Deng, Z.X., Bai, Y.F., Fu, X.Q.: Potential barrier-induced dynamics of finite energy Airy beams in fractional Schrödinger equation. Opt. Express **25**(26), 32560–32569 (2017)
33. Huang, X.W., Deng, Z.X., Fu, X.Q.: Dynamics of finite energy Airy beams modeled by the fractional Schrödinger equation with a linear potential. J. Opt. Soc. Am. B **34**(5), 976–982 (2017)
34. Chen, W.J., Wang, T., Wang, J., Mu, Y.N.: Dynamics of interacting Airy beams in the fractional Schrödinger equation with a linear potential. Opt. Commun. **496**, 127136 (2021)
35. Zhang, L.F., Zhang, X., Wu, H.Z., Li, C.X., Pierangeli, D., Gao, Y.X., Fan, D.Y.: Anomalous interaction of Airy beams

36. He, S.L., Malomed, B.A., Mihalache, D., Peng, X., He, Y.J., Deng, D.M.: Propagation dynamics of radially polarized symmetric Airy beams in the fractional Schrödinger equation. Phys. Lett. A **404**, 127403 (2021)
37. Bender, C.M., Boettcher, S.: Real spectra in non-Hermitian Hamiltonians having PT symmetry. Phys. Rev. Lett. **80**(24), 5243–5246 (1998)
38. Makris, K.G., El-Ganainy, R., Christodoulides, D.N., Musslimani, Z.H.: Beam dynamics in PT symmetric optical lattices. Phys. Rev. Lett. **100**(10), 103904 (2008)
39. Makris, K.G., El-Ganainy, R., Christodoulides, D.N., Musslimani, Z.H.: PT-symmetric optical lattices. Phys. Rev. A **81**(6), 063807 (2010)
40. Zhang, Y.Q., Zhong, H., Belic, M.R., Zhu, Y., Zhong, W.P., Zhang, Y.P., Christodoulides, D.N., Xiao, M.: PT-symmetry in a fractional Schrodinger equation. Laser Photonic Rev. **10**(3), 526–531 (2016)
41. Wu, Z.K., Yang, K.B., Zhang, Y.G., Ren, X.J., Wen, F., Gu, Y.Z., Guo, L.J.: Nonlinear conical diffraction in fractional dimensions with a PT-symmetric optical lattice. Chaos Soliton Fract. **158**, 112010 (2022)
42. Dong, L.W., Huang, C.M.: Vortex solitons in fractional systems with partially parity-time-symmetric azimuthal potentials. Nonlinear Dyn. **98**(2), 1019–1028 (2019)
43. Zhu, X., Yang, F.W., Cao, S.L., Xie, J.Q., He, Y.J.: Multipole gap solitons in fractional Schrödinger equation with parity-time- symmetric optical lattices. Opt. Express **28**(2), 1631–1639 (2020)
44. Zeng, L.W., Shi, J.C., Lu, X.W., Cai, Y., Zhu, Q.F., Chen, H.Y., Long, H., Li, J.Z.: Stable and oscillating solitons of PT-symmetric couplers with gain and loss in fractional dimension. Nonlinear Dyn. **103**(2), 1831–1840 (2021)
45. Li, P.F., Malomed, B.A., Mihalache, D.: Symmetry-breaking bifurcations and ghost states in the fractional nonlinear Schrödinger equation with a PT-symmetric potential. Opt. Lett. **46**(13), 3267–3270 (2021)
46. Chu, X.X., Liu, Z.J., Zhou, P.: Generation of a high-power Airy beam by coherent combining technology. Laser Phys. Lett. **10**(12), 125102 (2013)
47. Bloch, F.: Über die quantenmechanik der elektronen in kristallgittern. Z. Physik **52**(7–8), 555–600 (1929)